Charge Separation and Surface Reconstruction: A Mn^{2+} Doping Study†

Zoran V. Saponjic,* Nada M. Dimitrijevic, Oleg G. Poluektov, Lin X. Chen, Eric Wasinger, Ulrich Welp, David M. Tiede, Xiaobing Zuo, and Tijana Rajh*

Chemistry Division, Materials Science Division, Argonne National Laboratory, Argonne, Illinois 60439

Received: July 18, 2006; In Final Form: August 22, 2006

Hydrothermal synthesis of Mn doped anatase (TiO_2) nanoparticles using scrolled nanotubes of TiO_2 and $MnCl_2$ as the starting materials is described. Incorporation of Mn^{2+} ions on the substitutional sites was confirmed using X-ray absorption fine structure (FT-XAFS) while the oxidation state Mn(II) and coordination environment were determined using both electron paramagnetic resonance (EPR) and X-ray absorption near edge spectroscopy (XANES). Two different hyperfine couplings of 96 and 86 G were found using high-field (130 GHz) EPR reporting that Mn atoms occupy two distinct sites: one undercoordinated (reconstructed surface) and the other octahedral crystalline geometry (nanoparticle core), respectively. It was found that Mn atoms that occupy surface layers are weakly bound to the anatase lattice and can be easily leached using simple dialysis, while those incorporated in the nanoparticle core are bound more strongly and cannot be removed by dialysis. Light excitation EPR reveals that Mn ions incorporated in the surface layers participate in the charge separation, while those trapped deeply in the nanoparticle core do not show any photoactivity. Doping of the core of nanoparticles with Mn^{2+} ions, on the other hand, enables synthesis of optically transparent films having superparamagnetic behavior at room temperatures with a saturation magnetic moment of 1.23 μ_B per Mn atom.

Introduction

The inherent property of nanostructure materials is a large surface-to-bulk ratio. Typically the effect of the surface in nanocrystalline materials is treated with the simple model in which the abrupt termination of the nanoparticle surface results in broken bonds at the surface. This approach does not include alteration of the known band structure caused by the response of the surface structure to abrupt termination and ignores bonding reconstruction of surfaces. On the other hand, the properties of surface atoms that constitute a large fraction of the nanocrystalline system are affected by both the surrounding environment and the nanoparticle interior. The coordination sphere of the surface atoms is incomplete and causes readjustment of the crystalline structure to accommodate for the large surface area and high curvature of the nanoparticles causing the change in the local crystalline environment of the surface layers. In this size regime, the oscillator strength and energy of the band gap transitions can be significantly modified even if the energy levels are delocalized over the entire nanocrystal.

Recently, Friesner et al.[1] have shown that surface termination can change the internal electronic structure of silicon nanocrystals. Our group has previously reported that the large surface area and high curvature of metal oxide nanoparticles results in the change of crystalline symmetry of surface ions due to the reconstruction of nanoparticle surfaces.[2] We have shown that surface atoms in TiO_2 nanoparticles adopt an incomplete coordinate character resulting in the bond lengths and coordination environment of surface atoms that are distinct from those in the bulk and propagate five surface layers within nanoparticles.[3] In this work, we report the effect of the altered crystalline symmetry of reconstructed surfaces on the light-induced chemistry of TiO_2 nanoparticles. To understand the correlation between the coordination geometry and the thermodynamic parameters of lattice atoms, we investigated low-temperature electron transfer in surface and bulk doped TiO_2 nanoparticles using electron paramagnetic resonance (EPR) spectroscopy.

We use paramagnetic Mn^{2+} ions incorporated in the anatase lattice at substitutional sites within the surface or the bulk regions of nanoparticles as reporters of the coordination environment of the host anatase matrix. In addition, doping of wide band gap metal oxide semiconductors with transition metal atoms is important in its own right because it is expected that doping will influence the electronic, optical, catalytic, and magnetic properties of metal oxides. In particular, doping of metal oxide semiconductors such as ZnO and TiO_2 with paramagnetic atoms such as Mn is predicted to lead to interesting magnetic and magnetooptical behavior of nanoparticles resulting in room-temperature ferromagnetic transparent films.[4] Diluted magnetic oxides (DMOs) are attracting intense interest for potential new device applications in spin-based information-processing technologies because of the possibility of realizing compact and stable devices that could easily be addressed by external electrical and optical fields. Understanding the effects of nuclear spin provided by the paramagnetic dopant with photogenerated electrons in DMOs is in a core of yet unexplored opportunities for using carrier−dopant interactions in optical control of ferromagnetic behavior.[5] Significant improvements of magnetic properties of DMOs were reported when the size of host ZnO falls in the nanocrystalline regime.[6] Furthermore, the control of magnetization was achieved by surface modification of nanoparticles with electroactive ligands emphasizing the importance of the chemistry of surface termination on the internal electronic structure of dopant atoms.[5]

EPR is the method of choice for the study of structural details of the environment that incorporates paramagnetic dopants with

† Part of the special issue "Arthur J. Nozik Festschrift".

* To whom correspondence should be addressed. E-mail: Rajh@anl.gov.

10.1021/jp064548p CCC: $33.50
Published on Web 10/18/2006

respect to their chemical nature, oxidation state, and the local symmetry. In addition, due to the exchange interactions between paramagnetic ions and their nearest and distant neighbors, paramagnetic ions report on their electronic couplings with adjacent lattice atoms. Coupled with light excitation, EPR reveals the energetics and reactivity of selected atoms in the different environments. Herein, we find diverse hyperfine coupling and zero field splitting parameters of ^{55}Mn ions in the bulk and surface regions due to their different crystalline environment. X-ray absorption spectroscopy (XAS) was used to confirm coordination of incorporated Mn^{2+} ions, their oxidation state, and their positions within crystalline lattices, while wide-angle X-ray spectroscopy (WAXS) was used to interrogate the overall crystalline structure of doped nanoparticles. Using light excitation EPR, we find that, due to different crystalline environments, electronic coupling of Mn^{2+} ions with electronic states of TiO_2 nanoparticles in the surface and bulk regions are different: Mn^{2+} ions in the surface layers participate in light excitation processes, however those trapped deeply in the core of nanoparticles do not show any photoactivity. Photoactivity of Mn atoms in the surface region was explained by the change of transition probability (oscillator strength) due to deviation from the centrosymmetric crystalline environment of reconstructed surface layers. However, the presence of Mn^{2+} ions in the bulk region was found to contribute to the superparamagnetic behavior of nanoparticles at room temperature. These results suggest that while doping of the bulk region contributes to magnetic properties, doping of the surface region plays an important role in the primary events of charge separation and can be used for tuning the charge separation processes in nanoparticles.

Experimental Section

All chemicals were reagent-grade from Aldrich and used without further purification. Titania nanotubes were synthesized by using Degussa P25 TiO_2 powder as a precursor in a chemical process described elsewere.[7] Mn doped TiO_2 nanoparticles were synthesized using hydrothermal treatment of a suspension containing 3×10^{-2} M titania nanotubes at pH = 3 as the starting material in the presence of 6.3×10^{-3} M $MnCl_2$. The suspension was stirred for 4 h followed by a 60 min hydrothermal treatment at 250 °C. Nanoparticles were efficiently redispersed in water using a titanium ultrasonic horn (Branson Sonifier, 200 W), giving a transparent colloidal solution of Mn^{2+} doped TiO_2 nanocrystals. The sample was filtrated to remove excess Mn^{2+} ions, washed and redispersed in water pH = 3 (sample A), or dialyzed against water pH = 3 at 4 °C for 3 days (Sample B).

Apparatus. The size and shape of doped nanocrystals was determined using TEM, performed at the Electron Microscopy Center for Materials Research at Argonne National Laboratory (ANL). Specimens were imaged in a Philips CM 30 microscope operating at 100 kV. Wide-angle X-ray scattering (WAXS) data were collected at beamline 12 ID of the Advanced Photon Source (APS) at ANL. The X-ray was focused, and the spot size on the sample was ~1 mm × 0.5 mm. Data from wide-angle diffraction were presented in momentum transfer, q ($q = 4\pi \sin\theta/\lambda$, where θ is one-half of the scattering angle, and $\lambda = 0.67$ Å is the wavelength of the 20 keV energy probing X-ray), in the range 0−6 Å^{-1}. During the measurements, liquid dispersion of doped and undoped titania nanoparticles were held in a Suprasil cell. The X-ray absorption near-edge structure (XANES) and X-ray absorption fine structure (XAFS) data were collected at wiggler beamline 12 ID at APS. Si 111 crystals were used in the double-crystal monochromator. All spectra were collected at room temperature in the transmission mode. Samples of Mn^{2+} doped TiO_2 nanoparticles were ground into fine powders and sandwiched between two pieces of Kapton tape. MnO, Mn_2O_3, MnO_2, Mn(III) acetylacetonate, and Mn(II) acetylacetonate (Aldrich) were chosen as bulk references.

X-band (9.5 GHz) EPR experiments were conducted on a Bruker ESP300E spectrometer equipped with a standard Bruker rectangular cavity with optical access and a variable-temperature cryostat (Air Products). The microwave frequency was determined after each measurement using a Hewlett-Packard 5352B frequency counter. All samples were saturated with N_2 or Ar gas and illuminated using an Xe 300-W lamp. EPR measurements at high magnetic field were performed on a home-built pulsed/continuous-wave high-frequency D-band (130GHz/4.6T) EPR spectrometer[1,2] with a single mode cylindrical cavity TE_{011}. EPR spectra were recorded in the pulsed mode by monitoring the electron spin−echo intensity from a two/three microwave pulse sequence, as a function of magnetic field. The lengths of the microwave pulses were 40 and 80 ns. Pulses were separated by a time delay, τ, of 200 ns. The sample temperature was regulated by an Oxford temperature controller (ITC 503) coupled to an Oxford continuous-flow cryostat (CF 1200).[8,9]

The percentage ratio of Mn^{2+} ions to Ti^{4+} ions in doped nanoparticles was determined using the ICP technique with mass detection. Before the ICP measurements, the sample of Mn^{2+} doped TiO_2 nanoparticles was dissolved in 2 mL of concentrated sulfuric acid. The concentration of Mn^{2+} ions was 0.85% compared with the amount of Ti^{4+} ions.

Films for magnetic measurements are prepared by spin coating of dialized colloidal dispersion of Mn^{2+} doped TiO_2 onto a glass substrate. After each deposition of 20 μL of dispersion, the sample was annealed in air for 2 min at 200 °C. The field dependence of the magnetic moment of our samples was measured in a commercial SQUID (superconducting quantum interference device) magnetometer. The samples were mounted on a low-background sample holder with the film plane parallel to the applied field direction. The background magnetic signal was determined separately and subtracted from the sample measurements.

Results and Discussion

Manganese atoms were incorporated into titanium dioxide nanoparticles by a hydrothermal treatment of scrolled anatase nanotubes in the presence of manganese chloride. In our previous work, we have shown that scrolled TiO_2 nanotubes are shaped due to the presence of undercoordinated titanium sites that fold layers of anatase titania into scrolled nanotubes with large curvatures.[10] Scrolled nanotubes of TiO_2 contain large amounts (60%) of surface Ti atoms in highly reactive undercoordinated sites. The addition of manganese ions in high concentration (0.1 M $MnCl_2$) to scrolled nanotube precursors was found to unroll the nanotubes into sheetlike structures indicating a strong adsorption of manganese ions at undercoordinated sites that terminate layers of scrolled titanium dioxide nanotubes. Hydrothermal treatment of nanotubes containing Mn^{2+} adsorbed on undercoordinated sites was found to result in the formation of doped anatase nanoparticles having a rectangular shape with average dimensions of 10−12 nm. Upon 1% doping (sample A), the optical properties of nanoparticles slightly change, shifting the onset of absorption to ~450 nm. These nanoparticles also show weak photoluminescence at 490 nm. This result indicates that energy levels of Mn atoms incorporated into the TiO_2 lattice are located within the band

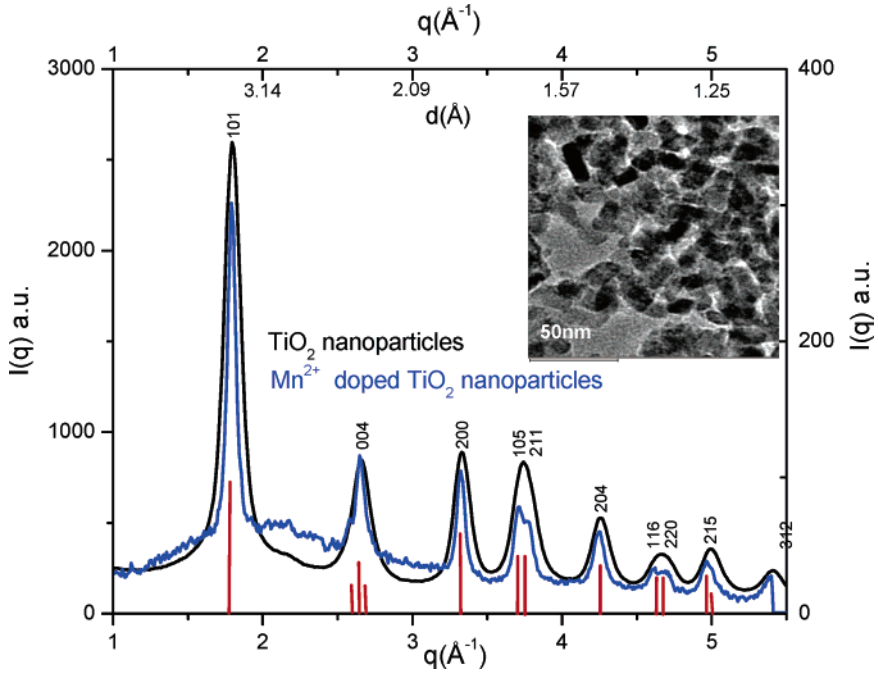

Figure 1. WAXS spectra of undoped TiO_2 anatase nanoparticles and Mn^{2+} doped TiO_2 nanoparticles. Inset: Transmission electron micrograph (or TEM image) of Mn^{2+} doped TiO_2 nanoparticles.

gap region and participate in the light-induced charge-transfer processes. Thorough dialysis of the 1% doped TiO_2 nanoparticles was used for removing manganese ions from weakly bound lattice sites within nanoparticles. Reoccurring dialysis led to the leaching of manganese ions to approximately 0.1%, when equilibrium was reached, leaving the residual manganese unchanged upon further dialysis (sample B).

WAXS shows the presence of a homogeneous anatase crystal structure in both samples (Figure 1). All diffraction features characteristic of the anatase lattice structure with preserved intensity ratios between them are present. In agreement with the low concentration of Mn dopant, there is no inhomogeneity raised by the presence of Mn^{2+} ions or indications of MnO clustering. However, while the presence of Mn^{2+} ions does not cause disturbance of the overall anatase structure, there is still a possibility of local distortions caused by incorporation of Mn^{2+} ions either at substitutional sites or at interstitial sites. Mn^{2+} ions are slightly larger and have a charge that is significantly different from that of the Ti atoms which constitute the anatase matrix.

The Mn K-edge XANES of sample B shows the edge position of Mn in the anatase nanoparticles close to those of divalent species, such as Mn(II) acetylacetonate (Mn(II)-acac), instead of higher valence species (Figure 2a). Hence, the valence of the Mn^{2+} ion is retained after its incorporation into the anatase nanoparticles. A slight shift of the edge position in the XANES spectrum is a possible perturbation of surrounding Ti(IV) that is more electron deficient than Mn(II), and can conceivably balance the electron distribution by shifting the electron density away from Mn(II), resulting in the edge shift to higher energy, as seen in Mn doped silica glasses.[11] However, comparison of the preedge structure in the spectra of Mn doped nanoparticles with that of MnO shows two completely different features of the two compounds although they share the same redox state and O_h coordination. It has been shown that the appearance of a peak at the transition edge (B) in MnO that is ~2 eV shifted from the Mn K-edge jump (peaking at 6.5470 keV) is a consequence of constructive and destructive interferences related to Mn distant neighbors 5−6.5 Å around central Mn atoms.[12] This feature is only vaguely present in Mn doped nanoparticles indicating a small contribution of Mn distant neighbors. Instead, a new feature ~6 eV shifted (6.5433 keV) from the Mn K-edge jump is observed that is not present either in Mn(II)-acac or in MnO model compounds (Figure 2b). The concomitant disappearance of the feature related to the Mn distant neighbors and the appearance of a new peak at the transition edge confirm successful incorporation of mainly isolated Mn^{2+} ions into TiO_2 nanoparticles with new electronic properties arising from the contributions of Ti distant neighbors located within a few angstroms from the central Mn dopant. It should be noted that the similar prepeak ~6 eV shifted from the Mn (III) K-edge jump was observed in the TiO_2 samples doped with Mn^{3+} ions.[13] Detailed characterization of the contribution of neighboring Ti atoms to the preedge structure using the Mn L-edge is currently underway.[13]

A detailed investigation of the Mn(II) coordination environment within the anatase lattice to demonstrate the effects of the bond distances and the location of the absorbing Mn was obtained using XAFS analyses. A reference structure of Mn-doped anatase with one Mn atom replacing one of the Ti atoms in a central location was constructed. The simulation was used as the Cartesian coordinates for the simulation using FEFF8.2. The single and multiple scattering paths from the calculation were used as a reference in fitting the experimental data. The fitting results and the structural parameters extracted from the fitting are shown in Figure 2c. The simulated spectrum that fits the best FT-XAFS experimental spectrum shows that the average Mn−O bond length is about 0.1−0.14 Å longer than the Ti−O bond lengths in anatase. The local distortion of the anatase lattice upon doping may be a consequence of a larger ionic radius of Mn(II) ions in octahedral coordination (0.97 Å for high spin and 0.81 Å for low spin)[14] compared to those of native Ti (IV) (0.74 Å) as well as charge compensation as a result of the lower oxidation state of Mn^{2+} compared to Ti^{4+}. However, the coordination numbers are not changed drastically from those in anatase lattice, indicating that the distortion caused by a mismatch between Mn^{2+} and Ti^{4+} is local and the lattice of anatase is retained upon Mn doping. However, the width of the

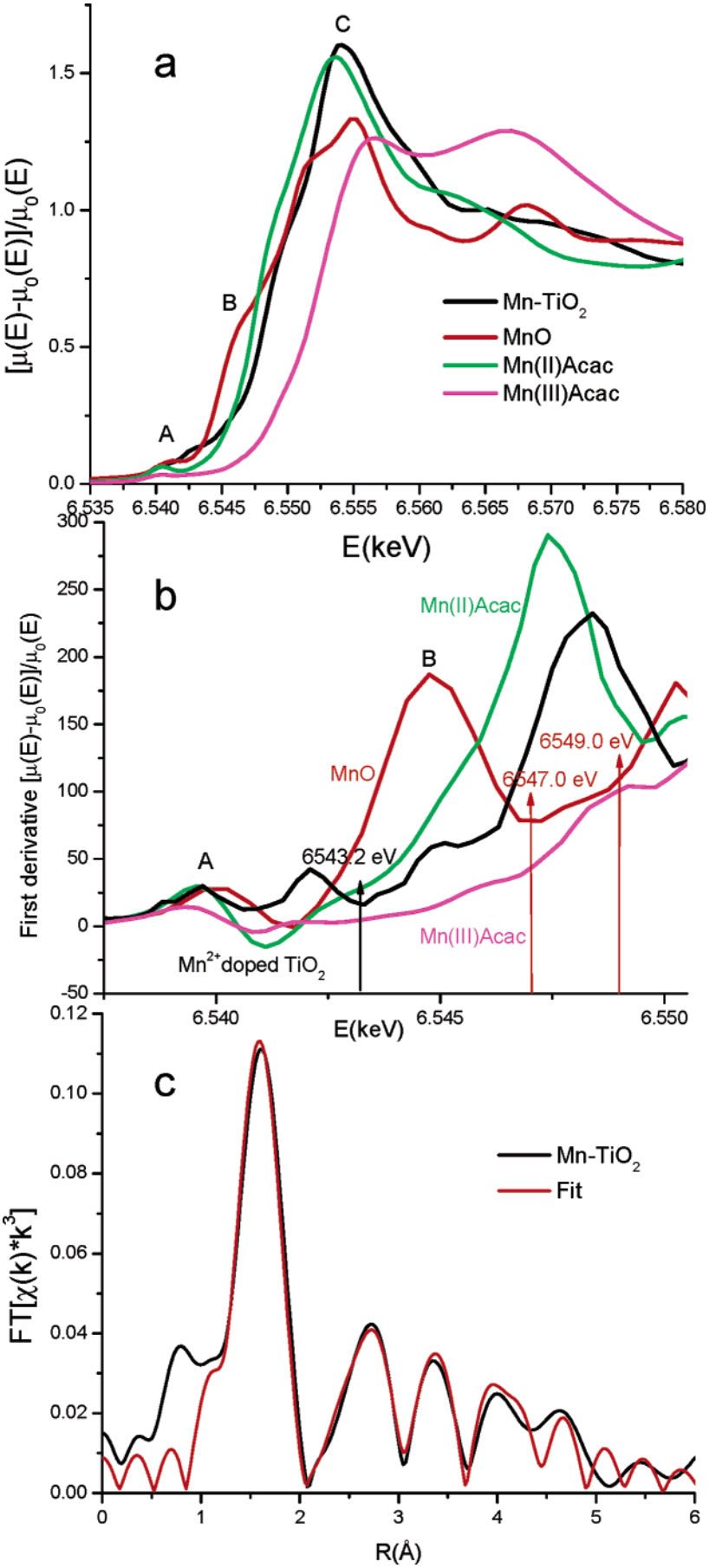

Figure 2. Mn K-edge XANES spectra of Mn^{2+} doped TiO_2 nanoparticles, MnO, Mn(II)-acac, and Mn(III)-acac (a), details of the preedge region presented as normalized first derivative of absorption where first derivative minima indicate characteristic peaks in the XANES spectrum (b), and experimentally obtained and simulated Mn K-edge EXAFS spectra (k^3-weighted) of Mn^{2+} doped TiO_2 nanoparticles (c).

peaks in the FT-XAFS spectrum of Mn-doped nanoparticles are significantly larger than those in the Ti K-edge FT-XAFS spectrum of anatase, and the Debye−Weller factors in the former are considerably larger than those metal oxide crystals at room temperature, suggesting that the local distortion caused by the replacement of Ti by Mn could propagate through the lattice beyond the nearest neighbors. There is no evidence of Mn clustering from XAFS data that would appear in the second shell arising from different Mn−Ti and Mn−Mn distances. In the case of Mn clustering, the higher Z (Mn) backscatterer would shift the maximum of the oscillation envelope to higher *k*, which was not found for Mn doped nanoparticles. It should be noted that doping of nanoparticles with Mn(III) did not cause local distortion of the crystalline lattice. Measured Mn−O and Mn−Ti distances in this case were comparable to Ti−O and Ti−Ti distances in the anatase that is in agreement with the comparable radii of Mn(III) (0.78 Å for high spin and 0.72 Å for low spin)[14] and Ti(IV) (0.74 Å) in octahedral environment.

EPR spectroscopy was used to confirm the presence of magnetically isolated Mn^{2+} dopants in the TiO_2 matrix and to investigate the interaction of photogenerated charge carriers with substitutional Mn atoms. Figure 3a shows the EPR spectrum of a filtrated sample of Mn^{2+} doped TiO_2 nanocrystals (Sample A). In the spectrum, one set of sextet lines dominates which is characteristic for hyperfine splitting (^{55}Mn nucleus, $I = 5/2$) with an A_{iso} constant of 90.8 G. This hyperfine splitting is characteristic of the Mn(II) oxidation state ($A_{Mn(II)} > A_{Mn(III)} > A_{Mn(IV)} > A_{Mn(V)}$).[11] The hyperfine structure spectrum corresponding to the m_s $|-1/2\rangle \leftrightarrow |1/2\rangle$ is superimposed on broad resonances of the fine structure of Mn^{2+} (d^5, $S = 5/2$) that are broadened due to their strong angular dependence. It should be noted that the fine structure of Mn^{2+} ions is infrequently observed due to the strong angular dependence resulting in broadening of the EPR signal. The fact that we have observed fine structure is a strong indication of the relative ordering between Mn dopants. The fine structure splitting indicates a zero field splitting parameter of $D = 350$ G (1.02 GHz or 4.3 μeV). This relatively large zero field splitting also causes unusually large second-order effects leading to variation of hyperfine splittings ranging from 67 G at the low-field end of the spectrum to 112 G at the high-field end of the spectrum compared to those determined in SrO and SiO_2 matrices.[15]

Upon illumination, a decrease of all spectral features associated with the manganese signal was observed while new peaks at $g = 1.990$ and $g = 1.960$ appeared; see Figure 3b. It has been shown previously that the illumination of bare anatase nanoparticles of TiO_2 at cryogenic temperatures leads to the trapping of photogenerated holes and electrons with characteristic EPR signals for anisotropic oxygen centered radicals at $g_x = 2.024$, $g_y = 2.0121$, and $g_z = 2.007$and Ti(III) at $g_\perp = 1.990$ and $g_{||} = 1.960$, respectively.[16] In Mn doped TiO_2 nanoparticles, trapping of photogenerated electrons and the consequent formation of Ti(III) were observed at the characteristic fields but formation of photogenerated holes was replaced with the partial disappearance of the Mn^{2+} signal (30% of the dark intensity). These results suggest that Mn^{2+} dopant atoms participate as electron-donating centers in the process of light excitation.

The mechanism of charge separation between Mn^{2+} ions incorporated in the crystal structure of TiO_2 and Ti(IV) was probed by obtaining the time profile of the EPR signal in an on−off illumination cycle; see Figure 3b inset. The signal for Mn was measured at the position of the first peak in the hyperfine structure of the Mn^{2+} EPR spectrum at the static field of 3078 G at 4 K. During the first second of the illumination process, the intensity of the Mn^{2+} signal decreased and held constant for the rest of the illumination time. In the dark, the Mn^{2+} signal returned to its original value as a conformation of the recombination of the majority of Mn(III) with photogenerated electrons. The same type of experiment was used for obtaining the time profile for the appearance of the $Ti(III)_{latt}$ signal at the static field position of 3348 G at 4 K; see Figure 3b inset. During this period of illumination, the build up of this signal appeared immediately, however with a smaller time constant and reached a plateau ~20 s after the light was turned on, indicating that there is an intermediate state contributing to the formation of $Ti(III)_{latt}$, most probably conduction band electrons that have a signal too broad to be observed by EPR.[17] A comparison of the intensities of Mn(II) and $Ti(III)_{latt}$ signals as a surface area under the integrated signals (4:1) indicates that only one-fourth of the concentration of photogenerated electrons are localized as $Ti(III)_{latt}$, while all photogenerated holes are localized as Mn(III). In addition, the rate of formation of thermalized $Ti(III)_{latt}$ is the same as that in the "bare" TiO_2 nanoparticles indicating that the same intermediate is involved in electron transfer. When the light was turned off, a sharp decay of half of the $Ti(III)_{latt}$ signal intensity was observed but the residual signal for the $Ti(III)_{latt}$ remained in the dark. As the EPR signal of Ti(III) lattices is much narrower compared to Mn(II) (250 vs 1000 G, respectively), the residual concentration of $Ti(III)_{latt}$ was too small to be compared with the amount of Mn ions that participate in charge separation. These results suggest that the majority of photogenerated electrons (Ti(III)) are formed either via fast hole trapping at Mn substitutional sites or via direct excitation of Mn dopant atoms according to the reaction

$$TiO_2{:}Mn(II) \overset{h\nu}{\rightleftharpoons} Mn(III) + xe_{cb}^{-} + (1-x)Ti(III)_{latt}$$

Note that Mn(III) ($S = 2$) formed during excitation is an ion with an even number of electrons and is usually not observed using conventional X-band EPR due to commonly large zero field splitting and/or fast relaxation times.[18]

Participation of Mn in light excitation suggests strong coupling of electronic states of Mn dopant atoms and TiO_2 lattice constituents. To confirm that these Mn atoms are incorporated in the TiO_2 lattice, we have investigated the samples in which Mn^{2+} ions (6.3×10^{-4} M, pH = 3) are deliberately adsorbed on TiO_2 nanoparticles prepared with the same method. We find that upon adsorption a less resolved EPR signal containing six-line hyperfine splitting was obtained. Broadening of the lines is the consequence of the angle dependence of the signal because of their different orientation of Mn^{2+} ions randomly adsorbed on surface binding sites. Importantly, upon illumination, no disappearance of the Mn^{2+} signal was found revealing that manganese ions solely adsorbed at the particles surface do not participate in the reaction with photogenerated carriers.

The high-field EPR D-band (130 GHz) however reveals that the hyperfine sextet of lines in sample A is actually formed of two sets of sextets with slightly different hyperfine splittings, indicating that two species in different coordination geometry contribute to the signal observed using X-band (Figure 3c). The first sextet of lines with a hyperfine splitting constant of $A_{iso} = 86$ G corresponds to the octahedral coordination of Mn^{2+} ions incorporated in the bulk TiO_2. Existence of the second sextet with a hyperfine splitting constant of $A_{iso} = 96$ G shows the presence of Mn^{2+} ions in undercoordinated geometry formed most probably as a result of simultaneous incorporation of Mn^{2+} within the surface of nanocrystals. Temperature dependence of

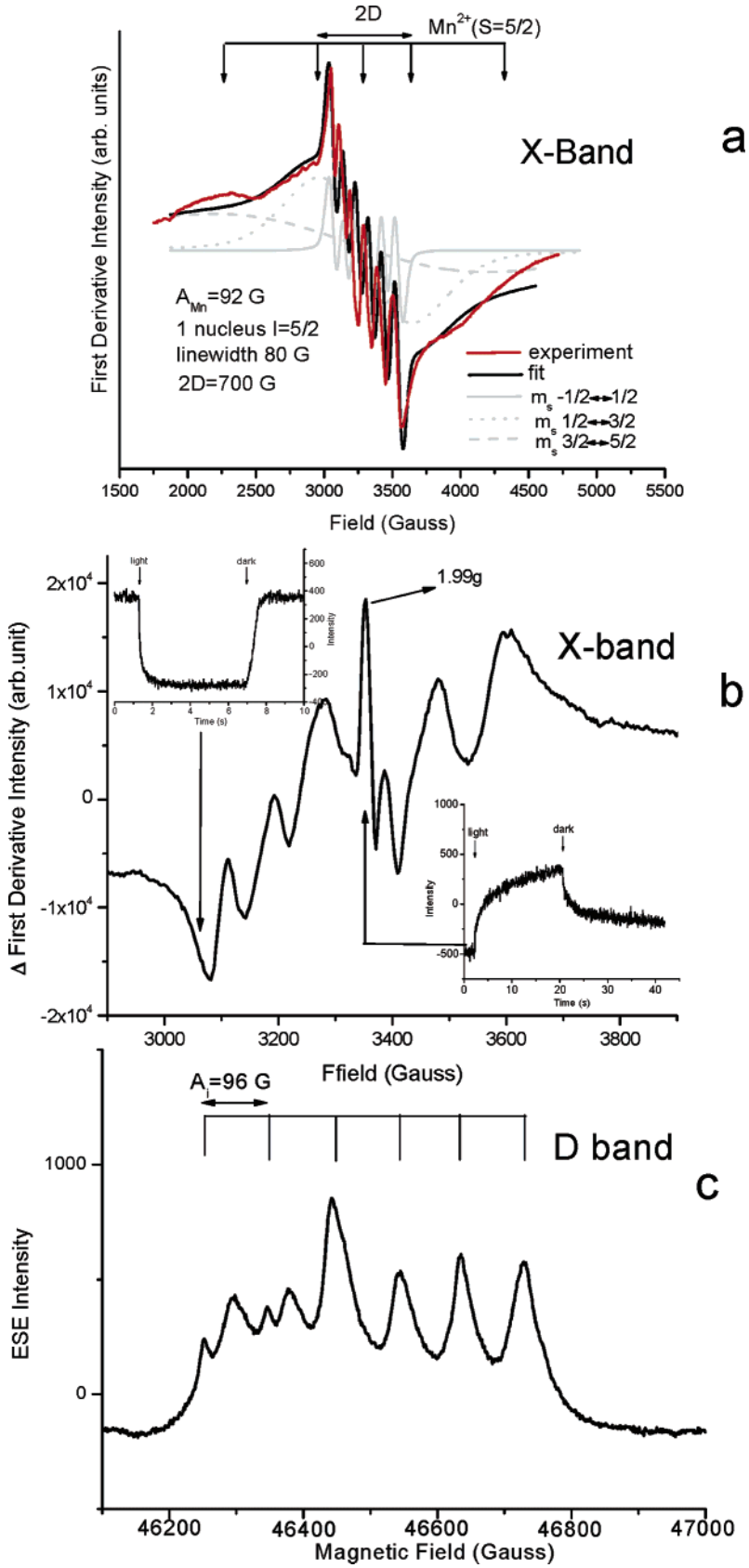

Figure 3. (a) Experimental and simulated X-band EPR spectra of Mn^{2+} doped TiO_2 nanoparticles, sample A; fine structure transitions were simulated separately due to different angle dependence that requires simulation with different line widths. Gray curves indicate simulated contributions between (S + 1) states: $m_s = -1/2$ to $1/2$, (solid), $m_s = 1/2$ to 3/2, line width (dot), and $m_s = 3/2$ to 5/2 (dash). The parameters used for fitting are indicated in the figure. The fitted curve was obtained by the addition of different contributions to the overall spectrum that fitted the best experimental data. The experimental spectrum was obtained using modulation amplitude (MA) of 6.3 G, time constant of 1.28 ms, and microwave power of 2 mW. (b) Light-induced changes in the EPR spectrum after illumination of sample A with Xe lamp (△ = light-dark). Insets: time profiles of the EPR signals in an on−off illumination cycle for decay of Mn signals recorded at low-field transition 3078 G (left top) and appearance of the $Ti(III)_{latt}$ signal recorded at 3348 G (right bottom). (c) High-field EPR D-band spectrum (130 GHz) of sample A.

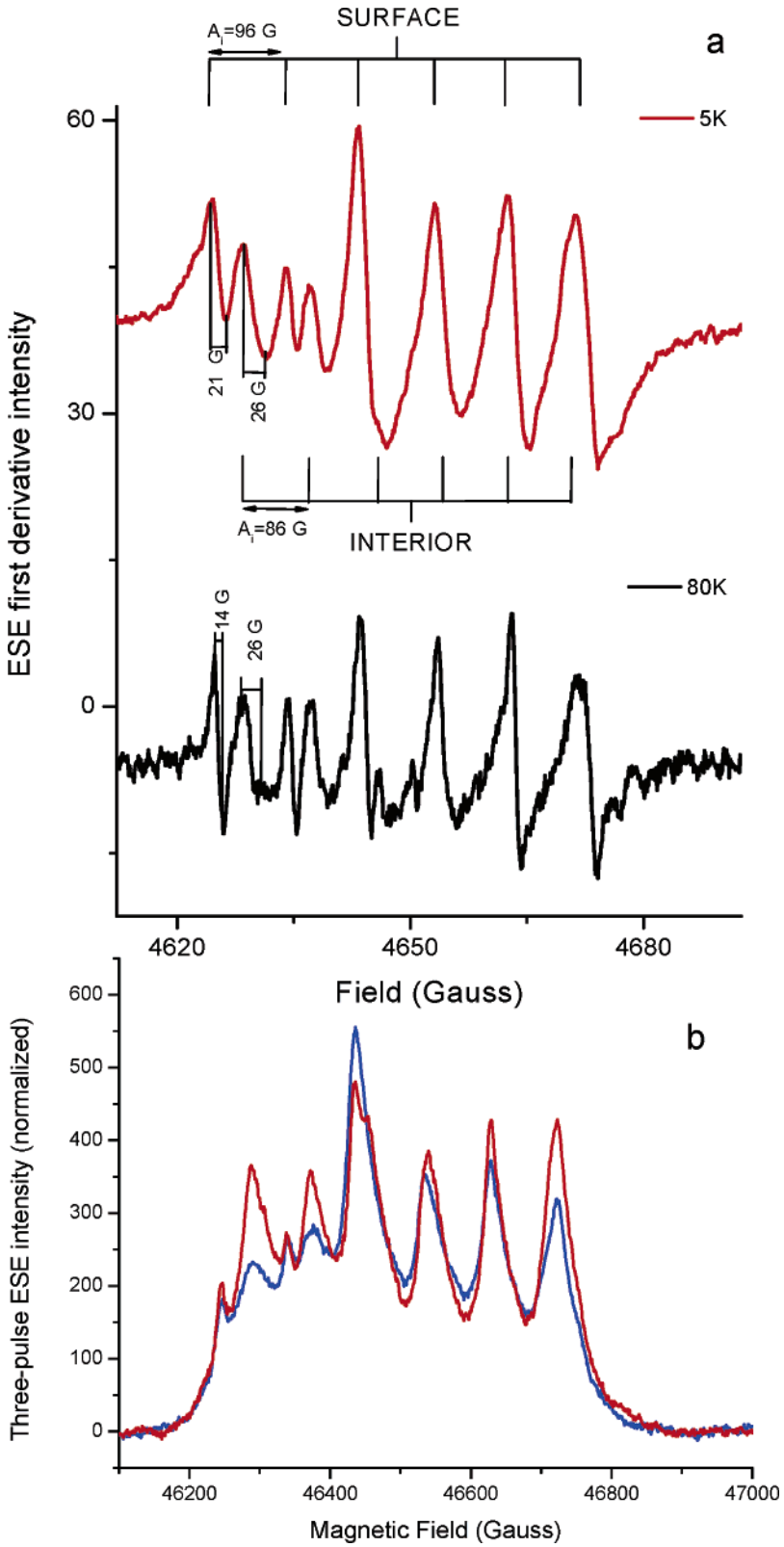

Figure 4. (a) High-field EPR D-band derivative spectra recorded at different temperatures of Mn^{2+} doped TiO_2 nanoparticles, sample A. (b) Saturation recovery three-pulse experiment, $\pi-T-\pi/2-\tau-\pi$ (π pulse was 40 ns, and τ time was fixed to 150 ns) recorded at 50 K of sample A. The red spectrum is recorded with a T time of 100 μs while the blue spectrum is recorded at T time equals 1.5 Φ s.

this signal (Figure 4) shows that the line width of the spectrum having the larger hyperfine constant decreases faster with temperature. This result indicates that the species in undercoordinated geometry within the surface relaxes much faster than the one having octahedral symmetry positioned in the core of the nanoparticles. Faster relaxation suggests stronger exchange interaction of Mn atoms in the reconstructed surface with an anatase host matrix that probably leads to the stronger coupling with electronic states of anatase lattice.

To further demonstrate the difference in the relaxation rates of the surface and core doped Mn atoms, we performed direct measurements of relaxation times T_2 and T_1 by pulsed EPR at

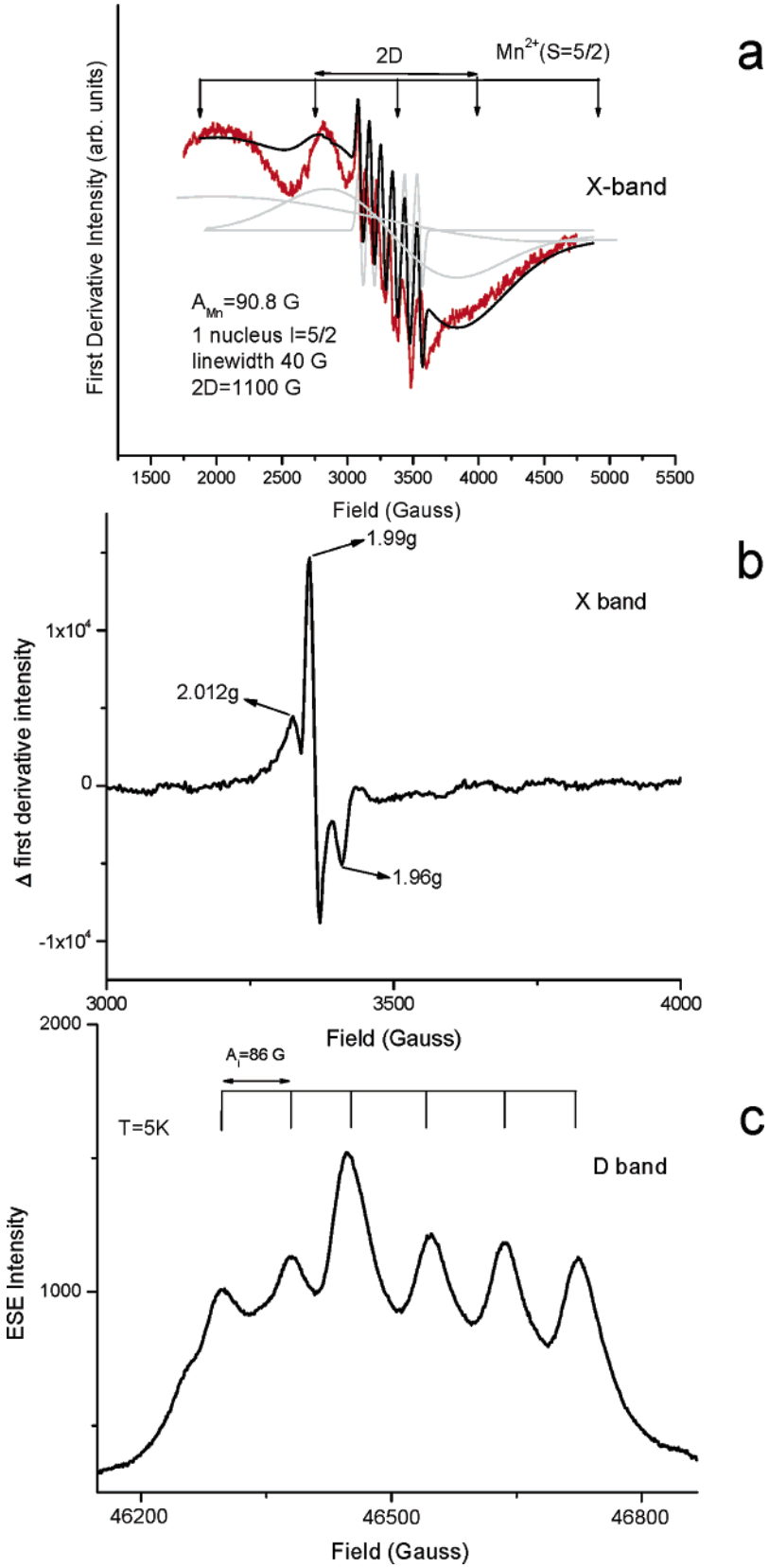

Figure 5. (a) Experimental and simulated X-band EPR spectra of Mn^{2+} doped TiO_2 nanoparticles, sample B; gray curves indicate simulated contributions between (S + 1) states: $m_s = -1/2$ to $1/2$, (solid), $m_s = 1/2$ to 3/2, line width (dot), and $m_s = 3/2$ to 5/2 (dash). The parameters used for fitting are indicated in the figure. The fitted curve was obtained by the addition of different contributions to the overall spectrum that fitted the best experimental data. The experimental spectrum was obtained using a modulation amplitude (MA) of 6.3 G, time constant of 1.28 ms, and microwave power of 2 mW. (b) Light-induced changes in the EPR spectrum after illumination with Xe lamp ($\triangle$ = light-dark) (sample B). (c) High-field EPR D-band spectrum (130 GHz) of sample B.

130 GHz. The T_2 time was measured by the two-pulse sequence ($\pi/2-\tau-\pi$) and T_1 time—by the saturation recovery three-pulse experiment ($\pi-T-\pi/2-\tau-\pi$). The τ time in the two-pulse experiment and the T time in the saturation recovery experiment

were varied. The length of the B-pulse was 40 ns, and the τ time in the three-pulse experiment was fixed to 150 ns. We did not observe any difference in the relaxation rates of both centers at low temperatures. Thus, at 10 K, $T_2 \approx 290$ ns and $T_1 \approx 7.5$ Φ s. However, with the increase in temperature, both centers demonstrate the same T_2 dependence ($T_2 \approx 170$ ns at 50 K), but the T_1 times are clearly different for these centers. Two field swept spectra recorded at 50 K in saturation recovery experiments are shown in Figure 4b. The red spectrum is recorded with a T time of 100 μs which is much longer than the T_1 time of the system ($\sim$2.4 Φ s). Therefore, this spectrum can be considered completely recovered. The blue spectrum is recorded at T time equals 1.5 Φ s, which is comparable to the T_1 time in the system. This figure clearly demonstrates that recovery of the surface Mn^{2+} lines is faster than that of the lines corresponding to the Mn doped in the core of the particles reporting that the T_1relaxation time of surface Mn is faster. This difference in the relaxation times is still small at 50 K, of the order of 20−40%, and can be observed only in the EPR line shape but not in the kinetics of the saturation recovery experiment.

The same type of EPR measurements was acquired for the dialyzed sample of Mn^{2+} doped TiO_2 nanoparticles, sample B (Figure 5c). Only one sextet of lines with a hyperfine splitting constant of $A_{iso} = 86$ G was observed indicating that only Mn^{2+} ions in anatase-like octahedral coordination are present in this sample. This experiment confirms that thermodynamically stable incorporation of Mn^{2+} ions in the anatase lattice that is resistant to a "self-purification" mechanism[19] occurs only by doping within the bulk region of the nanoparticle that is in octahedral symmetry.

Removal of Mn^{2+} ions using dialysis (sample B) resulted in the sharpening of the hyperfine features (line width decreases from 80 G in sample A to 40 G in sample B, see Figure 5a). Sharpening of the EPR signal reveals that those residual Mn atoms that are strongly bound in the nanoparticle core are oriented within the TiO_2 crystalline lattice decreasing the angular dependence of the EPR signal. In addition, the zero field splitting obtained from the fine structure of Mn^{2+} becomes 550 G (6.4 μeV, 1.5 GHz), significantly larger than that found in the surface layers. The difference in the zero field splitting comes from the different crystal fields that Mn^{2+} ions experience in the different crystalline environments of the surface and bulk regions. However, illumination of the sample that contains Mn^{2+} ions only within the bulk core in anatase octahedral symmetry does not have any effect on the EPR signal for Mn^{2+} ions (Figure 5b). Instead, the difference spectrum shows formation of species having the same spectrum as the one obtained upon illumination of "bare" TiO_2 anatase particles obtained by the same hydrothermal synthesis. In these rectangular shaped nanocrystals, formation of two characteristic species was observed: photogenerated holes with axially symmetric $g_\perp = 2.012$ and $g_\parallel = 2.007$ and photogenerated electrons with an axially symmetric signal having $g_\perp = 1.990$ and $g_\parallel = 1.960$. Therefore, illumination of bulk doped TiO_2 nanoparticles results in the excitation of electrons from the valence band of TiO_2 into the conduction band of TiO_2, and Mn atoms, although they occupy mid-gap states, they do not participate in charge separation processes. The observation that Mn atoms in octahedral symmetry do not participate in charge separation while those in undercoordinated surface sites do is consistent with the high symmetry of Mn atoms in anatase centrosymmetric geometry (D_{2d}). This in turn suggests that the atoms located within reconstructed surfaces of nanoparticles in noncentrosymmetric coordination environments are mostly involved in the light excitation process.

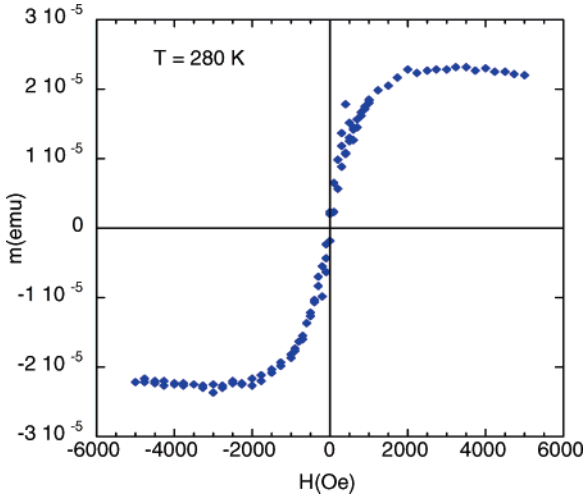

Figure 6. *m* vs H measurement at 280 K of spin-coated film made from Mn^{2+} doped TiO_2 nanoparticles, sample B.

The question that arises is whether those Mn^{2+} ions positioned in the core of nanoparticles contribute to enhanced superparamagnetism or ferromagnetism of doped nanoparticles. The high spin state of Mn(II) dopant atoms was confirmed using EPR spectroscopy. Recording of the EPR spectra at low temperature in the pulsed mode eliminates the distortion of the line shape due to saturation effects. The pulsed D-band (130 GHz) spectrum of Mn doped in TiO_2 nanoparticles shows a spectrum characteristic for high spin Mn atoms. The high spin of Mn^{2+} ions holds a promise for obtaining new transparent metal oxide based ferromagnetic semiconductors operating at room temperature.

For the measurement of the magnetic properties of Mn^{2+} doped TiO_2 nanoparticles, we prepared optically transparent thin films onto glass supports using a spin-coating technique. Annealing of the films provides better packing and connection between nanocrystals. It was shown that long-range magnetic ordering in aggregates of DMO nanocrystals correlates with the extent of aggregation.[20] Figure 6 shows the magnetization curve for the spin-coated Mn doped TiO_2 nanocrystalline thin film at 300 K. Upon doping, a large paramagnetic effect is observed at room temperature. The saturation magnetic moment of 1.23 μ_B per Mn atom was observed (total amount of Mn atoms present in the film was obtained using ICP). Magnetic properties of transition metal doped anatase TiO_2 were so far measured only in Co doped materials. Recently, Matsumoto et al.[21] have reported that Co doped anatase TiO_2 films exhibit magnetic domain structures characteristic of ferromagnetic long-range ordering with a saturated magnetic moment of 0.32 μ_B in which Co ions were in an apparently low spin state. Chambers et al.[22] have shown much larger saturation magnetic moments of 1.26 μ_B/Co and explained the enhancement of the magnetic moment by contribution of orbital moment in low spin Co atoms by an asymmetric crystalline field of $CoTiO_3$. On the other hand, doping with high-spin Mn^{2+} was predicted to have local magnetic moments of 3.0 μ_B due to the high spin state of Mn^{2+} ions (d^5) in which the spin down bonding of $t_{2g}^{\alpha}e_g^{1-\alpha}$ states led to the apparent d^3 spin state of Mn dopant atoms.[4] Doping of anatase TiO_2 nanoparticles with Mn using the hydrothermal method in this work is the first evidence of their superparamagnetic behavior. Surface modification with electroactive ligands[2] such as positively charged dopamine or negatively

TABLE 1: Structural Parameters for Mn^{2+} Doped TiO_2 Nanoparticles and Anatase TiO_2[a]

Mn^{2+}-doped anatase			anatase (calculated by FEFF8.2)		
N	*R* (Å)	σ^2 (Å^2)	N	*R* (Å)	σ^2 (Å^2)
6 (Mn−O)	2.07	0.009	4/2 (Ti−O)	1.93/1.97	0.004
4 (Mn−Ti)	3.16	0.010	4 (Ti−Ti)	3.03	0.004
8 (Mn−Ti)	3.87	0.0187	8 (Ti−Ti)	3.76	0.004
12 (Mn−O)	4.52	0.019	16 (Ti−O)	4.25	0.004
8 (Mn−O)	4.71	0.014	8 (Ti−O)	4.84	0.004

[a] *R*, bond distances; *N*, coordination numbers; and σ^2, static Debye-Weller factors.

charged 3,4-dihidroxyphenylacetic acid (dopac) did not have an effect on magnetization.

In summary, in this work, we have shown that hydrothermal synthesis of Mn doped anatase nanoparticles using titania scrolled nanotubes as the starting material results in successful incorporation of high-spin Mn^{2+} dopants in anatase nanoparticles. Mn^{2+} ions occupy two different sites having different binding energies: undercoordinated surface sites and core octahedral sites of TiO_2 nanoparticles. Mn atoms that substitute Ti atoms in the undercoordinated coordination environment of reconstructed surfaces are weakly bound to the anatase lattice and can be easily removed by "self-purification"[19] of nanoparticles during dialysis. These atoms however have electronic states strongly coupled to the band structure of TiO_2 nanoparticles and are primal participants in the light excitation processes. On the other hand, Mn atoms that substitute Ti atoms in the core of nanoparticles in the octahedral coordination environment are strongly bound to the anatase lattice and cannot be leached from nanoparticles. These dopants contribute strongly to the paramagnetic behavior of nanoparticles due to their slow relaxation, albeit only half of the theoretically predicted magnetization is observed. Three possible scenarios can be envisioned for the loss of magnetization: (i) exchange interaction between Mn atoms within the nanoparticle, (ii) absence of ordering of Mn atoms within the anatase crystalline lattice, or (iii) absence of long-range ordering of nanocrystals. As XAS studies show very weak exchange coupling between Mn atoms, and EPR studies show ordering of Mn atoms within the crystalline lattice resulting in observed fine structure of Mn atoms, we speculate that the absence of long-range ordering of TiO_2 nanoparticles is the cause of the loss of magnetization.

Acknowledgment. This work was supported by the U.S. Department of Energy, Office of Basic Energy Sciences, Division of Chemical Sciences under Contract W-31-109-Eng-38. The work benefited from the use of the Advanced Photon Source and Electron Microscopy Center for Materials Research at Argonne National Laboratory.

References and Notes

(1) Zhou, Z.; Brus, L.; Friesner, R. *Nano Lett.* **2003**, *3*, 163−167.

(2) Rajh, T.; Chen, L. X.; Lukas, K.; Liu, T.; Thurnauer, M. C.; Tiede, D. M. *J. Phys. Chem. B* **2002**, *106*, 10543. Redfern, P. C.; Zapol, P.; Curtiss, L. A.; Rajh, T.; Thurnauer, M. C. *J. Phys. Chem. B* **2003**, *107*, 11419−11427.

(3) Rabatic, B. M.; Dimitrijevic, N. M.; Cook, R. E.; Saponjic, Z. V.; Rajh, T. *Adv. Mater.* **2006**, *18*, 1033−1037.

(4) Park, M. S.; Kwon, S. K.; Min, B. I. *Phys. Rev. B* **2002**, *65*, 161209-(R).

(5) Liu, W. K.; Whitaker, K. M.; Kittilstved, K. R.; Gamelin, D. R. *J. Am. Chem. **Soc.*** **2006**, *128*, 3910. Kittilstved, K. R.; Norberg, N. S.; Gamelin, D. R. *Phys. Rev. Lett.* **2005**, *94*, 147209. Kittilstved, K. R.; Gamelin, D. R. *J. Am. Chem. Soc.* **2005**, *127*, 5292−5293.

(6) Sharma, P.; Gupta, A.; Rao, K. V.; Owens, F. J.; Sharma, R.; Ahuja, R.; Guillen, J. M. O.; Johannson, B.; Gehring, G. A. *Nat. Mater.* **2003**, *2*, 673−677;

(7) Kasuga, T.; Hiramatsu, M.; Hoson, A.; Sekino, T.; Niihara, K. *Adv. Mater.* **1999**, *11*, 1307.

(8) Lakshmi, K. V.; Reifler, M. J.; Brudvig, G. V.; Poluektov, O. G.; Wagner, A. M.; Thurnauer, M. C. *J. Phys. Chem. B* **2000**, *104*, 10445−10448.

(9) Poluektov, O. G.; Utschig, L. M.; Dubinski, A. A.; Thurnauer, M. C. *J. Am. Chem. Soc.* **2005**, *127*, 4049−4059.

(10) Saponjic, Z. V.; Dimitrijevic, N. M.; Tiede, D. M.; Goshe, A. J.; Zuo, X.; Chen, L. X.; Barnard, A. S.; Zapol, P.; Curtiss, L.; Rajh, T. *Adv. Mater.* **2005**, *17*, 965−971.

(11) Rakhimov, R. R.; Ries, H. R.; Jones, D. E.; Glebov L. B.; Glebova, L. N. *Appl. Phys. Lett.* **2000**, *76*, 751−753.

(12) Farges, F. *Phys. Rev. B* **2005**, 71, 155109.

(13) Wasinger, E.; et al. To besubmitted for publication.

(14) Shannon, R. D. *Acta Crystallogr. Sect. A: Found. Crystallogr.* **1976**, *32*, 751.

(15) Rosenthal, J.; Yarmus, L. *Rev. Sci. Instrum.* **1966**, *37*, 381.

(16) Rajh, T.; Ostafin, A. E.; Micic, O. I.; Tiede, D. M.; Thurnauer, M. C. *J. Phys. Chem. B* **1996**, *100*, 4538−4545.

(17) Berger, T.; Sterrer, M.; Diwald, O.; Knozinger, E.; Panayotov, D.; Thompson, T. L.; Yates, J. T., Jr. *J. Phys. Chem.* **2005**, *109*, 6061−6068.

(18) Rakhimov, R.; Jackson, E. M.; Jones, D. E.; Loutts, G. B. *J. Appl. Phys.* **2004**, *95*, 5653−5660.

(19) The "self-purification" mechanism was recognized as a reason for the high crystalline quality of nanocrystals that are easily annealed out due their small dimensions and diffusion lengths. The recent paper of Dalpian, G; Chelikowsky, J. R.; *Phys. Rev. Lett.* **2006**, *96*, 226802 considers thermodynamic arguments showing that the formation energy of defects increases with decreasing size of nanocrystals.

(20) Bryan, D. J.; Heald, S. M.; Chambers, S. A.; Gamelin, D. *J. Am. Chem. Soc.* **2004**, *126*, 11640−11647.

(21) Matsumoto, Y.; Murakami, M.; Shono, T.; Hasegawa, T.; Fukumura, T.; Kawasaki, M.; Ahmet, P.; Chikoyow, T.; Koshihara, S.; Koinuma, H.; *Science* **2001**, *291*, 854.

(22) Chambers, S. A.; Thevuthasan, S.; Farrow, R. F. C.; Marks, R. F.; Thiele, J. U.; Folks, L.; Samant, M. G.; Kellock, A. L.; Ruzycki, N.; Ederer, D. L.; Diebold, U. *Appl. Phys. Lett.* **2001**, *79*, 3467.